Velocity measurements with structured light transmitted through a multimode optical fiber using digital optical phase conjugation

LARS BÜTTNER,[*] **MARTIN THÜMMLER, AND JÜRGEN CZARSKE**

Technische Universität Dresden, Faculty of Electrical and Computer Engineering, Laboratory of Measurement and Sensor System Technique (MST), 01062 Dresden, Germany
[*]*lars.buettner@tu-dresden.de*

Abstract: Lensless fiber microendoscopes enable optical diagnostics and therapy with minimal invasiveness. Because of their small diameters, multimode fibers are ideal candidates, but mode scrambling hinders the transmission of structured light fields. We present the generation of a localized fringe system at variable distances from the distal fiber end by exploiting digital optical phase conjugation. The replayed fringe system was used for quantitative metrology. Velocity measurements of a microchannel flow in the immediate proximity of the fiber end without the use of any imaging lenses are shown. Lensless multimode fiber systems are of interest especially for biomedical imaging and stimulation as well as technical inspection and flow measurements.

1.   Introduction

Functional imaging and sensing of various physical quantities in deep tissue can provide essential information about the state of health of living organisms. An important example is the control of blood circulation deep inside the body, in particular for perfusion monitoring, atherosclerosis research [1], or for monitoring the cerebral blood flow in deep subcortical regions [2]. Optical measurement methods are in principle feasible of resolving the flow inside the tiny blood vessels with high spatial resolution down to the micrometer scale. However, light is subject to strong scattering within tissue, with a mean free path length (mean distance between two scattering events) in the range of only a few hundreds of micrometers. Optical coherence tomography (OCT), a non-invasive imaging method applied from outside the tissue is specialized to gain cross-sectional images of tissue, but is limited to application depths of a few millimeters [3]. For deeper penetration depths, scattering of light dominates more and more until the number of elastically scattered photons becomes too small to be detected. Hence, common optical measurement methods are limited to superficial applications.

In order to apply optical sensing deep inside the body, microendoscopes are currently being investigated for imaging, sensing and manipulation, which have diameters significantly smaller than 1 mm and can be inserted into tissue without significantly damaging it. Villiger *et al.* [3] presented a polarization-sensitive OCT system to differentiate malignant from benign tissue by means of birefringence for application in breast-tumor surgery. Its sample arm fiber was inserted in a needle probe of 570 μm outer diameter, enabling to record 3D images from deep within the tissue. Chen *et al.* [2] demonstrated blood flow measurements in the thalamus of mouse models using a 500 μm diameter microendoscope. They reported a significant change of the cerebral blood flow during acute hypoxia. Velocity measurements were based on laser speckle contrast imaging (LSCI) which uses the effect that the speckle pattern generated by the blood cells decorrelates on a time scale that is inverse proportional to the flow rate. Blood flow measurements in mouse cochlea have been reported as well [4]. LSCI, however, yields only relative changes of the flow rate and hence requires an extensive calibration, which has not been performed in-vivo yet. Moreover, the measurement is restricted to a single, fixed focal plane.

These problems can be solved by the use of structured light patterns. In many optical measurement methods, fringe patterns are the key to gain quantitative measurement information with low uncertainty. Some of these methods with a particular relevance for biomedical applications shall be mentioned in the following. Laser Doppler velocimetry (LDV) can measure local velocities of flows with low uncertainty (typ. 0.1% . . . 1%) and a spatial resolution in the order of typically 100 μm. Its measurement volume consists of system of nearly parallel interference fringes which are formed in the volume of intersection of two crossing coherent laser beams (two-beam interferometry) [5–7]. A derivate of this principle employs a Young's double-slit interferometer to generate fan-like interference fringes instead of parallel fringes. It enables direct measurement of the wall shear stress of wall-bounded flows, an important quantity in fluid mechanics [8] which is considered to play a key role in the understanding of the formation of atherosclerosis in blood vessels [1].

Other measurement methods based on structured light patterns are fringe projection for 3D shape recognition, structured illumination microscopy (SIM) for volumetric microscopy of biological samples with resolutions underneath the classical Abbe diffraction limit [9] and stimulated Brillouin scattering (SBS) for determining viscoelastic properties of biological tissue [10,11] or temperatures.

The desirable application of these measurement methods in deep tissue leads to the generalized problem of transmitting structured light patterns through microendoscopes. In order to reduce possible tissue damage to a minimum [12], it is self-evident that the diameter of such microendoscopes should be as small as possible. Classical endoscopes for investigations inside the human body usually employ fiber bundles (MCF: multi core fibers) as image guides, based on an array of single- or few-mode fibers. They are usually equipped with lenses at the distal end to accomplish the image transfer into the bundle. With typical diameters of several millimeters, they are unsuitable for insertion into sensitive tissue regions like the brain. On the other hand, single multimode fibers (MMF) have a significantly higher information density (about a factor of 10^1 . . . 10^2 when comparing the number of modes of an MMF with the number of cores of an MCF). Hence, because the diameter can be considerably smaller, MMFs are the ideal candidates for realizing microendoscopes [12,13]. The light field in MMFs is, however, subject to scattering processes as it propagates through the fiber which leads to mode conversion. The superposition of all excited modes generates a seemingly random, but actually deterministic speckle field at the fiber exit [14]. Together with biological tissue where light undergoes multiple scattering, these media are subsumed under the term "disordered media" in literature [15,16].

With the advent of spatial light modulators (SLM) with nowadays millions of degrees of freedom, optical wavefront shaping has emerged as a powerful tool to shape the wavefront approaching to the proximal multimode fiber facet appropriately such that a desired light field is obtained at the distal fiber end. The major task when applying these techniques is to find an appropriate phase or amplitude mask that compensates the distortion. Different approaches have been reported. In the iterative approach, the elements of the SLM are varied in a defined manner, e.g. on a Hadamard basis, such that a chosen metric, e.g. the intensity of a desired focal spot, gets optimized [15,17]. This approach requires only the evaluation of the intensity and hence no extra wavefront sensor is needed, but finding the global optimum is time consuming for modulators with restricted bandwidth or those with a high element count and may not always lead to unambiguous results.

Digital optical phase conjugation (DOPC) utilizes the time-invariance of the Maxwell equations. In a first step (calibration), the desired light field, the so-called guide star, is coupled into the distal end of the MMF and the light field emitted from the proximal side is measured by means of digital holography. In the second step (replay), the conjugated light field is generated by an SLM and guided backwards through the MMF such that the original light field of the guide star is reproduced at the distal end. Different realizations of guide stars have been reported, for

example fluorescent beads [18] or ultrasound waves [19] in biological tissue, or the Fresnel reflex at discrete phase boundaries [20]. A lateral scanning of the retrieved focal spot can be achieved by reprojecting different phase patterns [21] which has been demonstrated for imaging through MMF endoscopes [22,23].

At the matrix method [24,25], the impulse response from a single spot (or other basis functions) at the input is measured at the output, and this is repeated for all possible input sets, so that eventually the entire transmission matrix gets determined. Using the inverse matrix, any given light pattern at the distal end can be digitally reconstructed at the proximal end. The matrix method is hence predestined for transmitting images [13,25–27], but on the other hand it requires an extensive calibration procedure. Recently, machine learning approaches like deep neural networks are being investigated for image reconstruction through MMFs [28] as an alternative to wavefront shaping methods.

The vast majority of publications deals either with the transmission of Gaussian beam focal spots or with the recovery of two-dimensional images through MMFs. Recent works reported also on the formation of more complex, non-Gaussian beams with tailored point-spread functions and polarization states. Using DOPC or the matrix method with dedicated amplitude or phase masks, the transmission of Bessel beams [26,27,29] with increased depth of focus, donut beams with helical wavefronts [26,29,30], or radially polarized beams [27] through MMFs have been demonstrated.

In this contribution we show, for the first time to the best of our knowledge, the transmission of a localized, three-dimensional interference fringe pattern through an MMF for application in quantitative metrology. Because of its ability to determine the required phase mask in a single-shot rather than performing an extensive iteration or calibration process, DOPC was the method of choice here. It is the aim of this paper to show that multimode fibers can be used for lensless endoscopic light delivery of structured light patterns and to demonstrate its application for localized, quantitative measurements.

2. Experimental setup

A setup for digital optical phase conjugation as commonly reported in literature and based on the one in our previous publication [31] was realized to perform the experiments, see Fig. 1. The light of a solid-state laser (Coherent Verdi V5, wavelength $\lambda = 532$ nm) was launched into a single-mode optical fiber and guided to the experimental setup. The emitted beam was split by a polarizing beam splitter (PBS) into two paths of a Mach-Zehnder interferometer, one object path that forms the guide star and propagates through the multimode fiber (MMF), and a reference path. A half-wave plate placed before the PBS allowed for a tunable adjustment of the intensity splitting ratio between the two paths. Wavefront shaping was performed by a liquid-crystal phase-only spatial light modulator (SLM, HoloEye Pluto, 1920×1080 pixels, 8 µm pixel pitch) which is placed at the proximal side of the MMF.

During the calibration of the DOPC, the light that propagated through and is emitted from the proximal end of the fiber was superposed with the reference light on the SLM that was set uniform to a constant phase value during this step. The resulting light field was imaged onto CAM2 (CMOS, Ueye UI-348xLE0M, 2560×1920 pixels, 2.2 µm pixel pitch) which recorded an off-axis hologram.

For the flow measurements reported in Section 4, light power is a crucial issue. Hence, we reduced the number of involved beam splitters since every (non-polarizing) beam splitter induces power losses. A beam configuration was chosen where the reference beam illuminated the SLM under a defined inclination angle, see Fig. 1. To circumvent a too large inclination angle between the reference and the object beam at CAM2, the object beams were directed over an additional mirror M1 using beam splitter BS1, which was placed in the same imaging plane as the SLM with respect to CAM2.
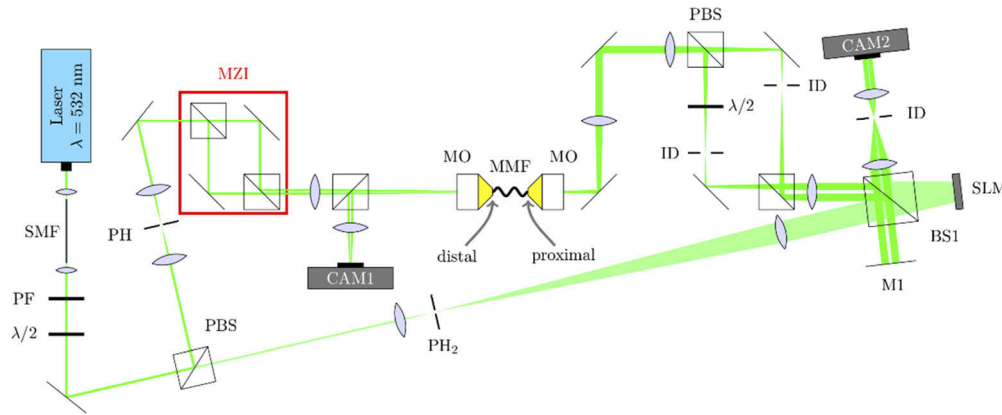
Fig. 1. Scheme of phase conjugation setup with polarization multiplex for the transmission of an interference fringe system through a multimode fiber. $\lambda/2$ – half-wave plate, BS – beam splitter, PBS – polarizing beam splitter, MO – microscope objective, MMF – multimode fiber, MZI – Mach Zehnder interferometer guide star, SLM – liquid crystal spatial light modulator, CAM – CMOS (Complementary metal–oxide–semiconductor) camera

For playback of the phase-conjugated light field, the light forming the guide star was blocked and the reference light was used to illuminate the SLM, which displayed the conjugated phase patterns. The modulated wave field propagates back through the MMF and forms the desired light field at the distal fiber end. The retrieved pattern is imaged via a magnifying Keplerian telescope onto CAM1 (CMOS, Ueye UI-306xCP-M, 1936 × 1216 pixels, 5.86 μm pixel pitch) for characterization. The employed multimode fibers were of the step-index type with a numerical aperture of NA = 0.22 and core diameters of D = 50 μm and D = 105 μm.

To achieve a better quality of the retrieved light field, a polarization multiplexing scheme was implemented in order to record and play back both polarization states [26]. The light emitted from the MMF was split by a polarizing beam splitter and guided onto two separate sub-windows of the SLM. A half-wave plate in one of the two beams rotated its polarization plane by 90° to account for the polarization properties of the liquid-crystal SLM. During playback, the two beams were modulated by their individual phase masks and combined by the same arrangement.

The guide star that was focused onto the distal fiber facet for the phase conjugation was either represented by a single focal spot or a fringe pattern. For adjustment of the setup and to perform basic tests of the phase conjugation, a single Gaussian beam was used. The fringe pattern used for the experiments described in the next section was generated by two-beam interferometry, realized by a Mach-Zehnder interferometer consisting of two non-polarizing prism beam splitters (BS) and two mirrors. The mirrors were aligned in such a way that the two partial beams intersected under a defined angle. After focusing the beams with a microscope objective onto the distal fiber end, the beams intersected under a half-angle of about $\theta \approx 6°$, resulting in a typical fringe spacing of $d = \lambda/(2sin\theta) \approx 2.5$ μm. The beam waists of the two partial beams were adjusted in such a way that they coincided with the crossing point of both beams. The profile and position of both types of guide stars were controlled by guiding the Fresnel reflex originating from the distal fiber facet via a beam splitter to CAM1 during calibration.

In order to prove the phase conjugation capability of the setup, first tests were carried out using a single focal spot of Gaussian profile with a $1/e^2$ radius of 2.5 μm as a guide star. A step-index multimode fiber with a fiber core diameter of D = 50 μm, a numerical aperture of NA = 0.22 and a length L = 1.5 m was employed, yielding a V-number of $V = \pi DNA/\lambda = 65$ and an estimate of the number of modes of $N \approx V^2/2 = 2112$. The replayed spot has a radius of 2.8 μm for all

polarization states (horizontal only / vertical only / both horizontal and vertical) what matches the size of the guide star quite well. The peak-to-background ratio (PBR) is about 230 for only one polarization state (239 for horizontal polarization, 217 for vertical polarization), whereas it is about 320 for both polarization states, which shows the benefit from the polarization multiplexing. These values did not reach the theoretical limit of phase-only phase conjugation reported in literature [32], $PBR_{theo} = N \cdot \pi/4 = 1659$, which is mainly due to the fact that the focal spot was not diffraction limited with respect to the fiber ($=d_{\mathrm{Diff}} \approx \lambda/(2NA) = 1.2\ \mu m$). Other reasons might be a limited alignment accuracy, decorrelation effects, optical aberrations or phase flicker of the liquid-crystal SLM [33]. The experiment, however, proves the functionality of the setup and the benefit of the polarization multiplexing.

3. Transmission of fringe systems

For first estimations of the transmission quality of a fringe system by means of DOPC, a numeric simulation was realized with general-purpose programming language Python including libraries NumPy and SciPy. It was conducted for step-index fibers, for one polarization direction and in Cartesian coordinates. It comprised the following three main steps: In a first step, the incident light field (guide star) was propagated through free space onto the distal fiber tip using the angular spectrum method, decomposed into the LP modes of the fiber (distal light field) and summarized as a vector. This input mode vector was multiplied with a transmission matrix to yield the output vector and the field at the proximal fiber tip. The transmission matrix was a random unitary matrix with non-vanishing secondary diagonal elements to describe mode mixing. In the second step, the replayed light field is defined by the proximal light field and under consideration of the playback conditions, e.g. a phase-only modulation. The third step is the backpropagation of the field through the fiber in the same manner as in the first step with the difference that now the inverse transmission matrix is used.

The guide star is represented by two coherent beams crossing under a small (half-) angle θ. We investigated the case that the guide star fringe system was not located on the fiber facet, but in a certain distance in front of it. From simulation shown in Figs. 2(a)–2(c) it is obvious that the DOPC is able to reproduce this situation during playback.
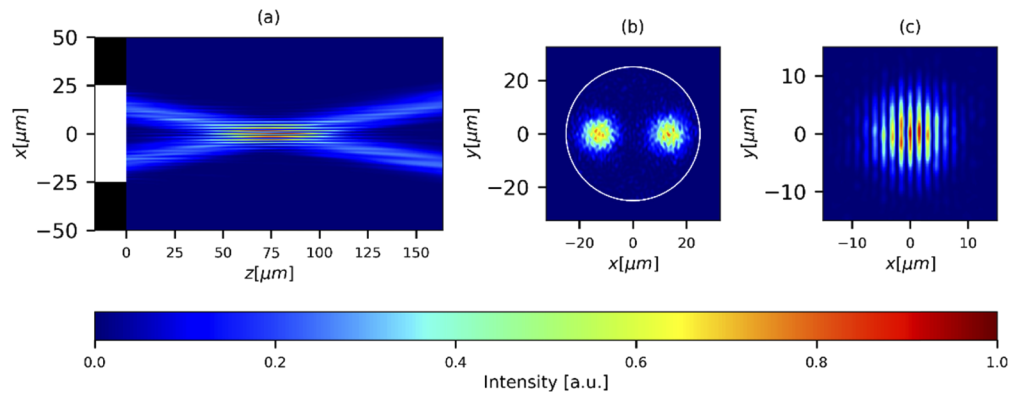

Fig. 2. Simulation of a phase-only conjugated light field emitted from a multimode fiber forming a localized two-beam interference fringe pattern with $\lambda = 532$ nm, D=50 μm, NA = 0.22, V = 65. (a) Light intensity in the direction of propagation (x-z-plane). The core of the MMF is represented by the white bar. (b) Intensity distribution on the fiber end facet at z = 0, showing the separated partial beams. (c) Intensity distribution in the center of the replayed fringe system at z = 75 μm.

As a result, the simulation proofs that it is possible to replay a *localized*, three-dimensional fringe system located at a certain distance with respect to the proximal fiber end by phase conjugation even without accounting for the amplitude for $V \gtrsim 20$. With regard to highly spatially resolved measurements using the fringe system the question for the minimum fringe spacing that can be transmitted through the MMF arises. It can be estimated based on the assumption that the two partial beams that generate the fringe system can have no larger inclination angle with respect to the fiber axis than the acceptance angle or numerical aperture of the fiber since they would not be able to virtually propagate within the fiber. This leads to the intuitive results that the minimum fringe spacing d_{min} corresponds to the mean radius of the fiber speckles $\bar{r}_{speckle}$:

$$d_{min} = \frac{\lambda}{2\sin\theta_{max}} = \frac{\lambda}{2NA} = \bar{r}_{speckle} \qquad (1)$$

We investigated the quality of the replayed fringe system in dependence of the fringe spacing with the simulation. Indeed, a sudden decrease of the fringe system quality can be noticed as the fringe spacing subsides the mean speckle radius, what confirms the hypothesis above.

Next, the transmission of a fringe system was investigated experimentally using the setup and the fiber (step-index MMF, D = 50 µm, NA = 0.22, L = 1.5 m) described in Section 2. Since a direct measurement of the replayed fringe system is hard to realize because of its proximity to the fiber facet, the fringe system was imaged into free space by the use of a Keplerian telescope. Its large magnification of 800/45≈17.8 allows for a direct recording of the replayed intensity distribution by means of CMOS camera CAM1. The results are shown in Figs. 3(a)–3(c). The images confirm the fringe system transmission as predicted by the simulation.

An electronic scanning along the optical axis can be realized. Different holograms were recorded for different positions of the guide star fringe system with respect to the facet of the distal fiber end. When playing back the corresponding conjugated phase masks on the SLM, a fringe system can be retrieved that is localized around a distinct and pre-defined position with respect to the fiber end. This is shown in the three columns of Figs. 3(a)–3(c), each representing a different position of the fringe system. The size and the position of the fringe system was characterized in more detail by scanning in small steps along the optical axis and determining the AC part of the pattern. It was calculated as the height of the corresponding spatial frequency from the spectrum of a perpendicular cross-section through the fringes. The result is displayed in Fig. 4 for four different phase masks. The fringe systems have an average length of 35 µm and consisted of about seven fringes. Note that this representation shows the actual z-scale, which was calculated back from the imaged fringe systems, with z = 0 being the estimated position of the distal fiber facet.

The scanning range is limited by the simple geometric consideration that the two partial beams generating the fringe system should not be separated on the fiber facet by more than the fiber core diameter to prevent truncation of the beams, see Fig. 2(a). Hence, it depends on the fiber parameters (core diameter and numerical aperture) and the parameters of the fringe system (lateral diameter, number of fringes). A large scanning range can only be achieved by decreasing the angle between the partial beams. This, however, would go along with a large fringe spacing and a low number of fringes, making it impractical for real applications. Hence, there is a trade-off between the scanning range and the number of fringes in the pattern. Using the numerical aperture NA = 0.22 of the employed fiber, we found that the scanning range is about 3D≈ 150 µm if a minimum of seven fringes in the pattern is presumed.
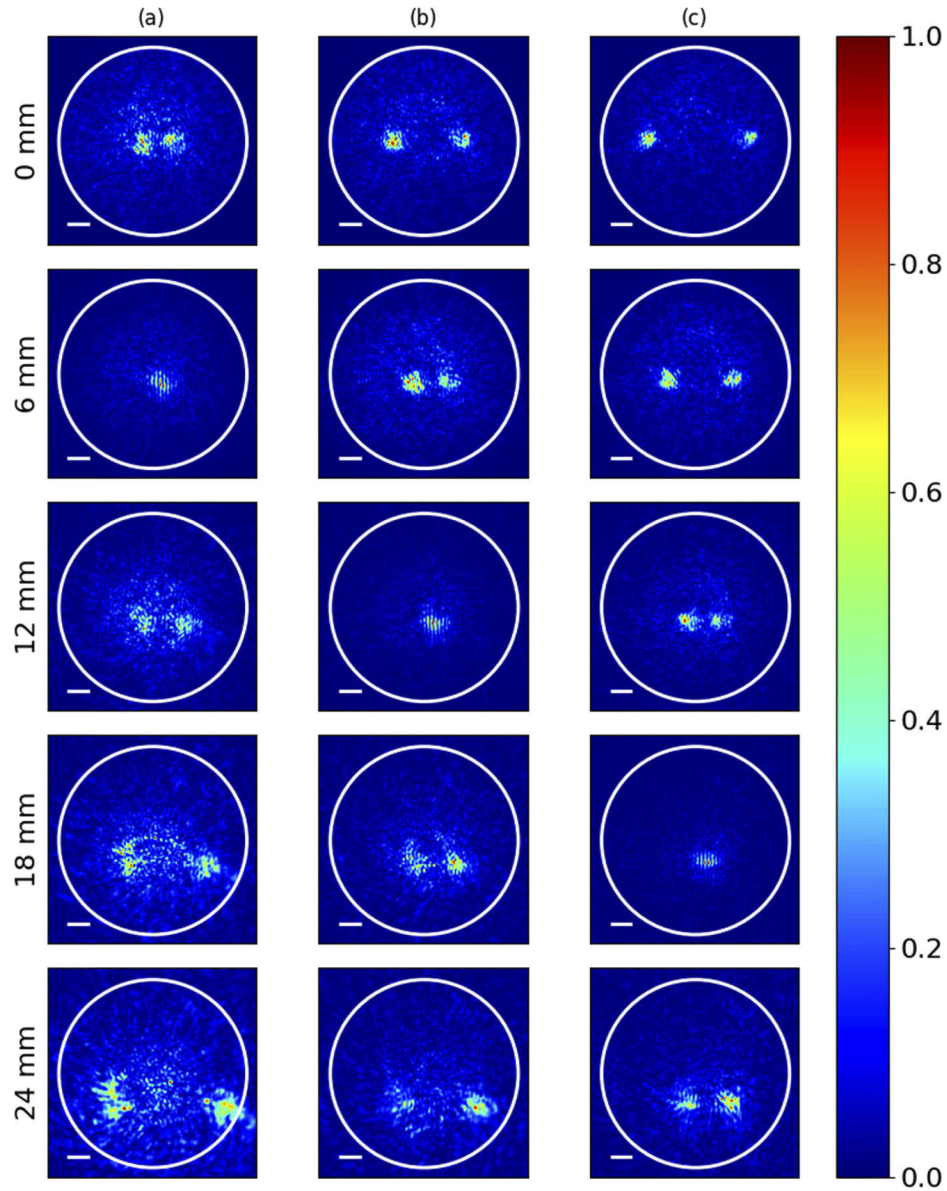
Fig. 3. Measured intensity distribution in five different axial planes at distance z for three different positions of the replayed fringe system. The light field emitted from the MMF (D = 50 μm, NA=0.22, L = 1.5 m) was magnified, imaged into free space and recorded with a camera. The white scale bar corresponds to 890 μm in the camera plane or 5 μm in the original imaged plane. The center of the fringe system is located (from left to right) at (a) z = 6 mm, (b) 12 mm, and (c) 18 mm.
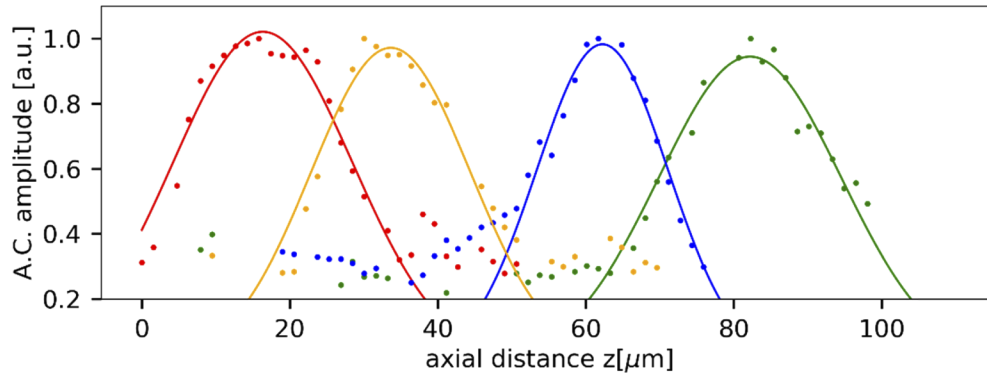
Fig. 4. Axial scanning of the localized fringe system by displaying different phase masks on the SLM. The plot shows the size and position of the fringe system by means of the AC part of the fringe system for four different phase masks that correspond to different distances of the fringe system with respect to the distal fiber facet(fiber parameters D = 50 µm, NA = 0.22, L = 1.5 m).

4.   Lensless velocity measurements of microchannel flow and discussion

As an example for lensless, localized measurements using a fringe system, a flow measurement is demonstrated at microchannel flow. The underlying principle for fringe-based velocity measurements is known as Laser Doppler velocimetry (LDV), a standard tool for measuring the flow profile of fluids. Here, scattering particles that are carried with the flow and that pass through the fringe system scatter light at the fringes of constructive interference. The scattered light is modulated in its amplitude with a distinct frequency that can be shown to be identical to the Doppler frequency f_D [5]. The velocity component perpendicular to the fringes can then be calculated by the Doppler frequency and the fringe spacing d as

$$v = f_D \, d. \tag{2}$$

We used a microchannel with an inner cross-section of 200 µm x 10 mm that was terminated to the top by a 180-µm-thick cover glass. The microchannel was placed upright such that the cover glass was facing towards the distal fiber end and the optical axis corresponds to the short dimension of the microchannel, see Fig. 6(a). It was placed in close proximity to the distal fiber end in a fixed position (estimated air gap between fiber end facet and cover glass ≈ 20 µm). Water was used as the working fluid. Fluorescent seeding particles (FluoMax, 2 µm mean diameter, maximum absorption at 500 nm, maximum emission at 610 nm) were added to the water to generate scattered light signals. The concentration was chosen low enough to ensure single particle scattering. The flow was driven by pump, resulting in a constant flow rate of Q = 100 µl/s, a Reynolds number of Re = 20 and hence a laminar flow regime. The light scattered from the particles was collected by a single lens, launched into a multimode fiber (D = 200 µm, NA = 0,22, L = 2 m length) and guided onto a photo detector. The mode dispersion of this receiving fiber does not affect the measurement since the entire transmitted power is registered by the photo detector and the measurement information is contained in the amplitude modulation. The electric burst signals were digitized and evaluated by a standard PC. A fast Fourier transform (FFT) was used to calculate the spectrum, and the Doppler frequency was estimated by fitting a Gaussian curve to the Doppler peak. A burst validation was implemented such that for averaging only those burst signals were taken into account whose peak-height-to-background ratio exceeded a certain threshold; other signals were discarded.

In order to cover the whole width of the channel during the measurement, the scanning range had to be extended, which can be achieved by using an MMF with a larger core diameter as shown in the previous section. Hence, an MMF with twice the diameter, D = 105 μm, NA = 0.22 and 300 mm length, was chosen for the phase conjugation to perform the flow measurements. For the calibration, all elements required for the generation of the fringe guide star were placed on an own breadboard, and phase masks for different positions of the fringe system guide star were recorded. After the calibration, this breadboard is brushed aside and another breadboard that contained the microchannel components is placed in front of the distal fiber end instead. The replayed fringe system had an approximate length of 100 μm and a fringe spacing of d = 2.4 μm. The optical power in the measurement volume was in the order of 1∼10 mW. Figures 5(a)–5(b) show a burst signal of a single scattering particle in the time (Fig. 5(a)) and in the frequency domain (Fig. 5(b)) as an example. It exhibits an obvious pedestal that results from the speckle background during replay. However, the interferometric visibility $V = (I_{max} - I_{min})/(I_{max} + I_{min})$ can be as high as 60%, resulting in a clear and distinct Doppler peak in the spectrum, see Fig. 5(b), which is high enough to be evaluated. The fringe system was scanned in steps of 25 μm through the channel and at each position about 10^4 burst signals were recorded and evaluated.
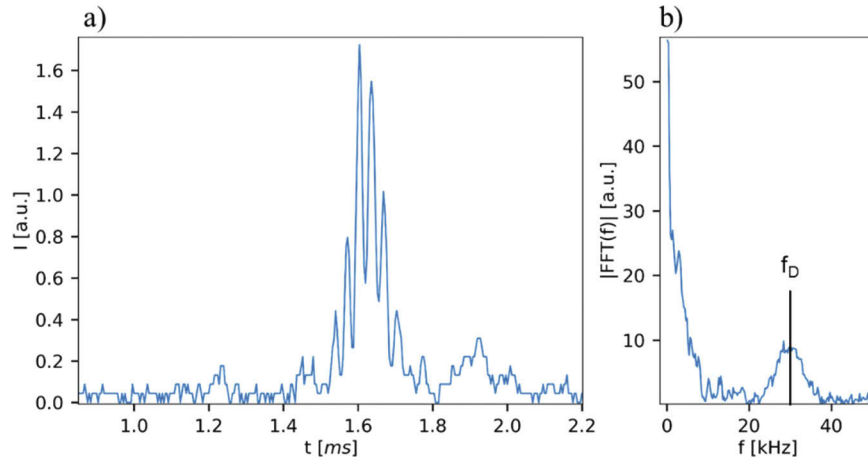

Fig. 5. Recorded photoelectric signal from a single scattering particle (a) in the time domain and (b) in the frequency domain as an example. Despite the remaining speckle background, the spectrum exhibits a clear peak (Doppler peak), whose center frequency is used to calculate the velocity of the particle.

The measured flow profile is shown in Fig. 6(b). The plot also contains the theoretical profile (dashed red line), which was obtained from $v(z) = 6Qz(W - z)/(H \cdot W^3)$ for a laminar flow condition. Here Q is the volume flow rate, W = 200 μm the width and H = 10 mm the height of the microchannel, and the expression is an approximation for rectangular channels with $H \gg W$. Since the measurement volume length is about half the channel width, the measurement suffered from a non-negligible spatial averaging effect leading to an apparent smoothing of the measured profile. Generally for LDV, the measured velocity profile $v_{meas}(z)$ is given by a convolution of the actual velocity profile present in the channel and the spatial response function $A(z)$ of the LDV, $v_{meas}(z) = v_{flow}(z) * A(z)$, where $A(z)$ is the AC part of the Doppler signal in the measurement volume, i.e. the amplitude of the Doppler peak, as shown in Fig. 4 as an example. With this, the expected profile was calculated and included as a green line in Fig. 6(b) as well. A good agreement is obtained for an averaging length of 50 μm and including a probabilistic averaging that took into account that burst signals with higher frequencies will be sampled more frequently [5].
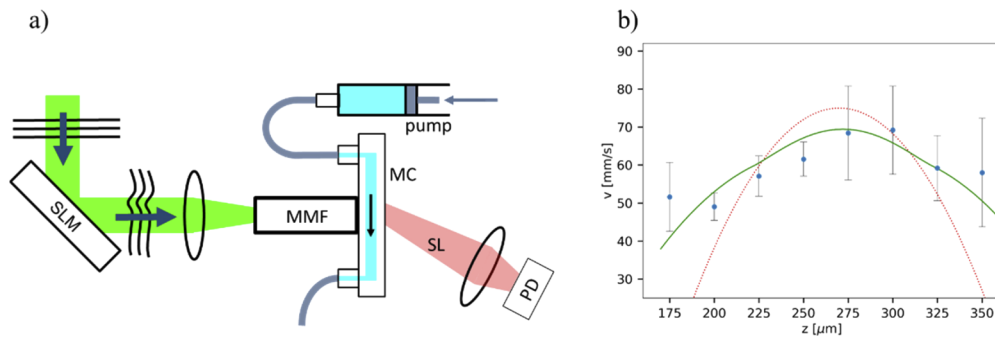
a)

b)

Fig. 6. Lensless velocity profile measurement of a microchannel flow. (a) Experimental setup (schematic, at the distal fiber end) for realizing a lensless velocity measurement in a microchannel. MMF: multimode fiber, SL: light scattered from seeding particles in the flow, PD: photo detector. (b) Flow velocity profile with z as the position with respect to the distal fiber facet. Blue dots: measurement. Red line: theoretical laminar flow profile estimated from the flow rate. Green line: expected velocity profile under consideration of the spatial averaging effect.

The spatial averaging gives also rise to an increased uncertainty of the velocity if a velocity gradient is present in the measurement volume as it was the case here. An ensemble measurement over stochastically distributed particles will yield a higher standard deviation than one with a flat velocity profile. Another uncertainty source is the moderate number of fringes since the uncertainty is inverse proportional to the period count when an FFT-based frequency estimator is used. Both effects are considered to be the main contributions to the uncertainty budget in the present setup.

In conclusion, the principle of measuring a flow profile could be successfully demonstrated and the flow velocity matches the estimated value. For future experiments, the spatial averaging effect can be reduced by using fringe patterns with a smaller lateral and axial extent. This can be achieved by choosing multimode fibers with a larger core diameter enabling larger crossing angles for extended working distances. The frequency estimation can be improved by using a period-independent frequency estimator like the quadrature demodulation technique.

5.   Summary and outlook

An approach for transmitting a fringe system through a multimode fiber using digital optical phase conjugation was presented. The fringe system can be generated in a certain distance with respect the distal fiber end and without using imaging lenses. Moreover, it is localized, i.e. it is of finite size in all three dimensions, which allows for spatially resolved measurements. Electronic scanning of the fringe system in axial direction can be realized by displaying different phase masks on the proximal spatial light modulator. The minimum transmittable fringe spacing corresponds to the mean speckle radius of the fiber.

As an example for quantitative measurements, a flow velocity measurement of a microchannel flow was presented, with the microchannel directly attached to the distal fiber end without using imaging optics. The measured flow profile agrees well with the one estimated from the flow rate. While the scattered light was collected in forward direction here, it can in principle be detected in backward direction and guided back through the same multimode fiber. This will enable a single optical access to the measurement location by only the MMF.

The presented work can pave the way towards the realization of lensless microendoscopes for application in deep tissue or other hard-to-access environments. To circumvent the necessity of repeated calibration in case of a fiber bending, the multimode fiber can be encapsulated in a

needle to prevent it from bending [3,34]. Alternatively, the employment of gradient index fibers can be considered. Recent works gave evidence that graded-index fibers are more robust against bending deformations [23,35].

As a perspective, the results can be of interest in a generalized context for various quantitative measurement principles that take advantage of structured light patterns.

Disclosures

The authors declare that there are no conflicts of interest related to this article.

References

1. P. Vennemann, R. Lindken, and J. Westerweel, "In vivo whole-field blood velocity measurement techniques," Exp. Fluids **42**(4), 495–511 (2007).
2. M. Chen, D. Wen, S. Huang, S. Gui, Z. Zhang, J. Lu, and P. Li, "Laser speckle contrast imaging of blood flow in the deep brain using microendoscopy," Opt. Lett. **43**(22), 5627–5630 (2018).
3. M. Villiger, D. Lorenser, R. A. McLaughlin, B. C. Quirk, R. W. Kirk, B. E. Bouma, and D. D. Sampson, "Deep tissue volume imaging of birefringence through fibre-optic needle probes for the delineation of breast tumour," Sci. Rep. **6**(1), 28771 (2016).
4. T. H. Kong, S. Yu, B. Jung, J. S. Choi, and Y. J. Seo, "Monitoring blood-flow in the mouse cochlea using an endoscopic laser speckle contrast imaging system," PLoS One **13**(2), e0191978 (2018).
5. H. Albrecht, M. Borys, N. Damaschke, and C. Tropea, *Laser-Doppler and phase-Doppler measurement techniques* (Springer, 2002).
6. L. Büttner, J. Czarske, and H. Knuppertz, "Laser-Doppler velocity profile sensor with submicrometer spatial resolution that employs fiber optics and a diffractive lens," Appl. Opt. **44**(12), 2274–2280 (2005).
7. L. Büttner, C. Leithold, and J. Czarske, "Interferometric velocity measurements through a fluctuating gas-liquid interface employing adaptive optics," Opt. Express **21**(25), 30653–30663 (2013).
8. A. A. Naqwi and S. Petrik, "Fiber-optic dual-cylindrical wave sensor for measurement of wall velocity gradient in a fluid flow," Appl. Opt. **32**(30), 6128–6131 (1993).
9. R. Heintzmann and T. Huser, "Super-Resolution Structured Illumination Microscopy," Chem. Rev. **117**(23), 13890–13908 (2017).
10. C. W. Ballmann, Z. Meng, A. J. Traverso, M. O. Scully, and V. V. Yakovlev, "Impulsive Brillouin microscopy," Optica **4**(1), 124–128 (2017).
11. B. Krug, N. Koukourakis, and J. W. Czarske, "Impulsive stimulated Brillouin microscopy for non-contact, fast mechanical investigations of hydrogels," Opt. Express **27**(19), 26910–26923 (2019).
12. S. A. Vasquez-Lopez, R. Turcotte, V. Koren, M. Plöschner, Z. Padamsey, M. J. Booth, T. Čižmár, and N. J. Emptage, "Subcellular spatial resolution achieved for deep-brain imaging in vivo using a minimally invasive multimode fiber," Light: Sci. Appl. **7**(1), 110 (2018).
13. D. Loterie, S. Farahi, I. Papadopoulos, A. Goy, D. Psaltis, and C. Moser, "Digital confocal microscopy through a multimode fiber," Opt. Express **23**(18), 23845–23858 (2015).
14. M. Plöschner, T. Tyc, and T. Čižmár, "Seeing through chaos in multimode fibres," Nat. Photonics **9**(8), 529–535 (2015).
15. I. M. Vellekoop, A. Lagendijk, and A. P. Mosk, "Exploiting disorder for perfect focusing," Nat. Photonics **4**(5), 320–322 (2010).
16. A. P. Mosk, A. Lagendijk, G. Lerosey, and M. Fink, "Controlling waves in space and time for imaging and focusing in complex media," Nat. Photonics **6**(5), 283–292 (2012).
17. C. Stockbridge, Y. Lu, J. Moore, S. Hoffman, R. Paxman, K. Toussaint, and T. Bifano, "Focusing through dynamic scattering media," Opt. Express **20**(14), 15086–15092 (2012).
18. X. Tao, O. Azucena, M. Fu, Y. Zuo, D. C. Chen, and J. Kubby, "Adaptive optics microscopy with direct wavefront sensing using fluorescent protein guide stars," Opt. Lett. **36**(17), 3389–3391 (2011).

19. Y. M. Wang, B. Judkewitz, C. A. Dimarzio, and C. Yang, "Deep-tissue focal fluorescence imaging with digitally time-reversed ultrasound-encoded light," Nat. Commun. **3**(1), 928 (2012).

20. H. Radner, L. Büttner, and J. Czarske, "Interferometric velocity measurements through a fluctuating phase boundary using two Fresnel guide stars," Opt. Lett. **40**(16), 3766–3769 (2015).

21. I. N. Papadopoulos, S. Farahi, C. Moser, and D. Psaltis, "Focusing and scanning light through a multimode optical fiber using digital phase conjugation," Opt. Express **20**(10), 10583–10590 (2012).

22. I. N. Papadopoulos, S. Farahi, C. Moser, and D. Psaltis, "High-resolution, lensless endoscope based on digital scanning through a multimode optical fiber," Biomed. Opt. Express **4**(2), 260–270 (2013).

23. A. M. Caravaca-Aguirre and R. Piestun, "Single multimode fiber endoscope," Opt. Express **25**(3), 1656–1665 (2017).

24. S. M. Popoff, G. Lerosey, R. Carminati, M. Fink, A. C. Boccara, and S. Gigan, "Measuring the transmission matrix in optics: An approach to the study and control of light propagation in disordered media," Phys. Rev. Lett. **104**(10), 100601 (2010).

25. S. Turtaev, I. T. Leite, T. Altwegg-Boussac, J. M. P. Pakan, N. L. Rochefort, and T. Čižmár, "High-fidelity multimode fibre-based endoscopy for deep brain in vivo imaging," Light: Sci. Appl. **7**(1), 92 (2018).

26. T. Čižmár and K. Dholakia, "Exploiting multimode waveguides for pure fibre-based imaging," Nat. Commun. **3**(1), 1027 (2012).

27. P. Yu, Q. Zhao, X. Hu, Y. Li, and L. Gong, "Tailoring arbitrary polarization states of light through scattering media," Appl. Phys. Lett. **113**(12), 121102 (2018).

28. N. Borhani, E. Kakkava, C. Moser, and D. Psaltis, "Learning to see through multimode fibers," Optica **5**(8), 960–966 (2018).

29. C. Ma, J. Di, Y. Zhang, P. Li, F. Xiao, K. Liu, X. Bai, and J. Zhao, "Reconstruction of structured laser beams through a multimode fiber based on digital optical phase conjugation," Opt. Lett. **43**(14), 3333–3336 (2018).

30. A. Boniface, M. Mounaix, B. Blochet, R. Piestun, and S. Gigan, "Transmission-matrix-based point-spread-function engineering through a complex medium," Optica **4**(1), 54–59 (2017).

31. J. W. Czarske, D. Haufe, N. Koukourakis, and L. Büttner, "Transmission of independent signals through a multimode fiber using digital optical phase conjugation," Opt. Express **24**(13), 15128–15136 (2016).

32. I. M. Vellekoop and A. P. Mosk, "Phase control algorithms for focusing light through turbid media," Opt. Commun. **281**(11), 3071–3080 (2008).

33. S. Turtaev, I. T. Leite, K. J. Mitchell, M. J. Padgett, D. B. Phillips, and T. Čižmár, "Comparison of nematic liquid-crystal and DMD based spatial light modulation in complex photonics," Opt. Express **25**(24), 29874–29884 (2017).

34. J. Li, E. Schartner, S. Musolino, B. C. Quirk, R. W. Kirk, H. Ebendorff-Heidepriem, and R. A. McLaughlin, "Miniaturized single-fiber-based needle probe for combined imaging and sensing in deep tissue," Opt. Lett. **43**(8), 1682–1685 (2018).

35. D. E. Boonzajer Flaes, J. Stopka, S. Turtaev, J. F. de Boer, T. Tyc, and T. Čižmár, "Robustness of Light-Transport Processes to Bending Deformations in Graded-Index Multimode Waveguides," Phys. Rev. Lett. **120**(23), 233901 (2018).